Supplementary Information for

Distinct hydrologic response patterns and trends worldwide revealed by physics-embedded learning

Table of Contents

Supplementary Tables

Table S1 | Mean Annual Runoff (mm/year) and corresponding water export quantities (in the parentheses, units of 10^9 tons/year) from different GWMs for 33 mixed-anthropogenic-impact large rivers.

Note: In Tables S1 and S2, we only evaluated and compared the simulations with observations when observational data were available.

GRDC Station ID	River	Observation	GWM1	GWM2	GWM3	GWM4	GWM5	δHBV2
01147010	Congo	341.98 (1183.2)	588.45 (2034.91)	512.74 (1779.59)	475.34 (1644.52)	360.15 (1246.1)	421.51 (1460.6)	541.98 (1891.7)
01159100	Orange	6.30 (5.56)	81.11 (70.60)	13.94 (12.35)	64.69 (56.71)	3.02 (2.63)	57.65 (50.2)	10.33 (9.24)
01834101	Niger	59.79 (121.83)	135.92 (274.5)	138.08 (279.29)	120.54 (243.06)	65.51 (132.65)	108.77 (220.68)	93.41 (187.4)
02906900	Amur	201.64 (354.52)	300.36 (523.87)	185.66 (323.67)	180.52 (313.63)	127.96 (223.89)	209.70 (366.72)	139.86 (251.72)
03629000	Amazon	1077.37 (5071.9)	1196.14 (5613.53)	1097.82 (5172.64)	1018.52 (4792.44)	948.73 (4469.4)	814.25 (3832.7)	1007.64 (4797.6)
03638050	Xingu	575.64 (256.29)	985.62 (437.04)	948.09 (419.26)	913.12 (402.39)	747.99 (331.46)	558.43 (244.51)	729.33 (328.88)
03650481	Parnaiba	70.84 (22.87)	308.64 (99.63)	222.97 (71.98)	269.47 (86.99)	107.54 (34.72)	124.53 (40.2)	107.64 (34.75)
03651805	Sao Francisco	319.61 (64.41)	586.05 (118.6)	492.73 (99.77)	451.59 (91.02)	361.16 (73.74)	503.76 (102.26)	355.90 (73.65)
03667060	Paraguai	196.79 (92.42)	493.57 (231.9)	364.25 (170.21)	360.93 (169.43)	295.46 (137.98)	421.17 (197.83)	321.07 (154.35)
04115200	Columbia	269.37 (166.37)	331.65 (203.61)	242.66 (149.52)	218.42 (134.34)	134.32 (83.19)	181.04 (111.49)	258.86 (161.52)
04127800	Mississippi	194.35 (581.09)	356.37 (1065.09)	191.13 (572.71)	254.41 (760.79)	166.44 (493.78)	279.03 (835.49)	196.47 (600.24)
04143550	Saint Lawrence	311.59 (240.77)	612.44 (474.93)	337.56 (261.7)	240.72 (186.92)	510.75 (395.41)	270.89 (209.94)	402.02 (319.86)
04152450	Colorado	48.85 (14.15)	121.35 (35.12)	63.30 (18.07)	102.90 (29.23)	11.18 (3.19)	78.35 (22.63)	80.40 (23.5)
04207900	Fraser	393.13 (85.77)	468.82 (102.0)	398.26 (86.95)	275.62 (59.91)	253.20 (55.55)	296.79 (64.61)	398.28 (87.71)

04208150	Mackenzie	150.40 (240.7)	231.80 (367.84)	195.70 (313.21)	107.46 (174.26)	114.59 (183.86)	127.45 (203.91)	133.67 (216.56)
04213550	Saskatchewan	48.33 (16.82)	182.79 (63.47)	104.22 (36.08)	136.72 (47.19)	54.73 (18.95)	95.40 (33.05)	66.20 (23.39)
04213650	Assiniboine	8.60 (1.35)	144.58 (22.32)	68.77 (10.61)	155.02 (23.77)	21.48 (3.34)	47.89 (7.47)	19.89 (3.14)
04213680	Red River of The North	45.95 (4.94)	194.76 (20.57)	80.91 (8.54)	161.92 (16.96)	47.37 (5.05)	88.62 (9.4)	42.48 (4.59)
04213800	Winnipeg	221.68 (28.33)	445.45 (56.67)	209.91 (26.58)	177.55 (22.63)	266.59 (33.95)	183.16 (23.43)	214.63 (27.83)
04214260	Churchill	86.48 (19.73)	317.32 (73.22)	213.40 (49.5)	104.29 (24.14)	149.12 (34.3)	1.93 (0.45)	111.18 (26.21)
04214520	Albany	232.30 (27.68)	534.76 (63.36)	382.26 (45.12)	301.08 (35.76)	366.60 (43.25)	220.44 (26.18)	288.37 (35.04)
04355100	Grande De Santiago	38.75 (5.0)	232.71 (29.88)	126.43 (16.17)	151.38 (19.39)	13.95 (1.78)	221.92 (28.51)	57.03 (7.44)
05101200	Burdekin	56.86 (7.5)	212.50 (27.62)	81.49 (10.85)	165.81 (21.75)	39.97 (5.11)	63.38 (8.31)	83.02 (11.04)
05101301	Fitzroy	30.97 (4.36)	217.47 (29.75)	50.78 (7.06)	170.33 (23.54)	24.37 (3.18)	84.86 (11.69)	57.62 (8.08)
05204250	Darling	4.40 (2.35)	194.85 (100.17	31.29 (16.32)	115.18 (59.62)	14.70 (7.72)	75.36 (38.91)	53.86 (27.63)
05410100	Cooper	5.08 (1.24)	170.73 (40.16)	18.97 (4.57)	96.75 (22.98)	19.59 (4.47)	24.39 (5.78)	99.77 (23.7)
06340110	Elbe	167.56 (21.64)	378.97 (49.71)	252.82 (33.16)	272.99 (35.91)	193.31 (25.2)	418.91 (54.97)	188.74 (25.26)
06435060	Rhine	464.82 (74.44)	724.87 (116.37)	570.48 (91.58)	572.19 (91.87)	556.97 (89.08)	654.42 (104.92)	500.00 (81.7)
06442600	Danube	352.47 (73.19)	569.48 (119.03)	398.80 (83.11)	405.38 (84.78)	370.39 (77.19)	537.88 (112.33)	403.51 (85.38)
06955430	Neva	283.41 (80.37)	525.45 (149.22)	446.98 (126.87)	316.99 (89.9)	342.68 (97.24)	134.17 (38.45)	323.60 (94.02)
06970250	Severnaya Dvina	301.46 (105.72)	441.36 (154.37)	421.58 (147.91)	299.40 (104.7)	324.29 (113.29)	104.91 (37.0)	288.67 (103.65)

06977100	Volga	190.92 (260.18)	357.10 (484.78)	287.70 (392.23)	289.90 (393.68)	204.08 (276.0)	183.42 (248.62)	201.27 (280.53)
06978250	Don	58.18 (22.02)	230.92 (86.58)	173.85 (65.69)	228.47 (85.49)	59.42 (22.09)	258.63 (96.41)	56.53 (21.78)
Summed value		(9258.71)	(13240.25)	(10902.87)	(10349.70)	(8728.74)	(8849.65)	(10029.09)
Bias			(3981.54)	(1644.16)	(1090.99)	(-529.97)	(-409.06)	(770.38)

Table S2 | Mean Annual Runoff (mm/year) and corresponding water quantities (units of 10^9 tons/year) from different GWMs for 28 natural basins.

GRDC Station ID	River	Observation	GWM1	GWM2	GWM3	GWM4	GWM5	δHBV2
01159103	Orange	5.31 (4.57)	79.43 (68.31)	13.83 (11.89)	61.10 (52.54)	2.98 (2.56)	57.00 (49.02)	10.19 (8.76)
02469260	Mekong	531.23 (289.52)	736.68 (401.49)	669.32 (364.78)	617.81 (336.71)	424.69 (231.46)	555.21 (302.59)	449.12 (244.77)
02646200	Ganges	361.45 (305.9)	646.40 (547.05)	562.43 (475.98)	593.97 (502.68)	389.63 (329.75)	519.95 (440.04)	342.29 (289.68)
02906700	Amur	163.96 (267.25)	300.79 (490.28)	192.24 (313.35)	180.86 (294.8)	124.90 (203.59)	216.03 (352.12)	113.26 (184.62)
02906901	Amur	202.32 (362.16)	310.91 (556.53)	193.04 (345.54)	190.34 (340.71)	141.52 (253.32)	222.40 (398.1)	155.62 (278.56)
02909150	Yenisey	246.23 (600.76)	233.24 (569.11)	248.25 (605.74)	190.56 (464.97)	179.83 (438.79)	200.16 (488.4)	237.64 (579.85)
02909152	Yenisey	192.12 (338.12)	207.05 (364.41)	211.55 (372.33)	148.59 (261.52)	127.44 (224.3)	165.37 (291.05)	181.92 (320.17)
02909153	Yenisey	169.27 (236.97)	175.47 (245.65)	184.29 (258.0)	118.62 (166.07)	88.68 (124.15)	163.28 (228.6)	161.87 (226.62)
02911097	Irtysh	42.78 (64.17)	102.67 (154.01)	83.99 (125.99)	109.11 (163.67)	29.72 (44.58)	100.00 (150.0)	45.77 (68.66)
02911100	Irtysh	30.27 (23.28)	49.43 (38.01)	38.11 (29.31)	59.73 (45.93)	9.68 (7.45)	88.71 (68.22)	23.98 (18.44)
02912600	Ob'	136.64 (403.07)	218.58 (644.81)	201.44 (594.25)	185.64 (547.65)	130.05 (383.66)	152.06 (448.56)	135.63 (400.11)
02912602	Ob'	111.49 (299.9)	195.99 (527.21)	180.21 (484.76)	172.01 (462.71)	105.58 (284.0)	135.89 (365.54)	110.35 (296.85)
03206720	Orinoco	1233.23 (1030.98)	1321.96 (1105.16)	1279.73 (1069.85)	1130.67 (945.24)	1080.01 (902.89)	1295.09 (1082.69)	1323.00 (1106.03)

03264500	Parana	489.16 (476.93)	772.74 (753.42)	552.16 (538.36)	527.36 (514.18)	520.36 (507.35)	683.87 (666.77)	494.93 (482.55)
03617110	Mamore	441.60 (268.9)	741.62 (451.64)	606.75 (369.51)	597.69 (363.99)	409.48 (249.37)	491.27 (299.18)	411.51 (250.61)
03635035	Madera	654.70 (713.54)	912.98 (995.15)	802.49 (874.72)	757.92 (826.13)	581.62 (633.97)	620.17 (675.99)	592.30 (645.61)
03635040	Madera	650.55 (634.87)	896.90 (875.38)	772.05 (753.52)	734.15 (716.53)	556.07 (542.73)	624.49 (609.5)	568.95 (555.29)
03649900	Tocantins	448.30 (327.76)	797.09 (582.89)	696.52 (509.35)	640.15 (468.12)	556.66 (407.07)	609.44 (445.67)	490.31 (358.55)
03649901	Tocantins	474.78 (327.97)	890.58 (615.32)	773.65 (534.53)	712.92 (492.57)	627.15 (433.31)	681.33 (470.74)	519.47 (358.91)
03649950	Tocantins	477.98 (354.77)	863.47 (640.95)	751.41 (557.77)	693.91 (515.09)	609.81 (452.66)	650.17 (482.62)	537.84 (399.24)
04103200	Yukon	246.26 (204.74)	186.01 (154.64)	225.39 (187.39)	164.40 (136.68)	154.63 (128.56)	134.91 (112.16)	178.66 (148.54)
04103550	Yukon	210.52 (107.03)	163.39 (83.07)	210.83 (107.19)	149.50 (76.01)	133.79 (68.02)	121.25 (61.65)	166.40 (84.6)
04115201	Columbia	312.52 (207.9)	388.35 (258.4)	292.35 (194.52)	268.51 (178.66)	182.93 (121.72)	266.74 (177.48)	325.41 (216.52)
04122900	Missouri	66.61 (90.43)	185.53 (251.89)	78.57 (106.68)	140.09 (190.2)	48.81 (66.26)	137.76 (187.03)	69.66 (94.57)
04122901	Missouri	53.33 (69.16)	166.29 (215.65)	67.08 (86.99)	126.46 (163.99)	38.34 (49.72)	127.86 (165.81)	58.45 (75.79)
04123050	Ohio	495.26 (260.38)	685.27 (360.29)	417.41 (219.46)	473.44 (248.92)	376.47 (197.94)	454.16 (238.78)	468.91 (246.54)
04127503	Mississippi	112.64 (203.33)	242.57 (437.9)	118.65 (214.2)	175.51 (316.83)	103.11 (186.15)	202.00 (364.65)	114.40 (206.52)
06542510	Danube	301.23 (158.38)	508.70 (267.48)	334.64 (175.96)	369.78 (194.44)	283.42 (149.03)	442.54 (232.69)	389.66 (204.89)
Summed value		(8632.74)	(12656.10)	(10481.92)	(9987.54)	(7624.36)	(9855.65)	(8351.85)
Bias			(4023.36)	(1849.18)	(1354.80)	(-1008.38)	(1222.91)	(-280.89)

Table S3 | Spatial R^2 values of different hydrologic signatures at the monthly scale.
The monthly hydrologic signatures were calculated for each basin, and their R^2 values were computed spatially across 28 natural rivers. Note that the slope of FDC was calculated based on the 1% and 33% exceedance probabilities, and only stations with at least 80% data availability were considered reliable for this calculation. The lag in parentheses after ACF indicates the number of lagged months used to calculate the autocorrelation function. The following metrics were calculated from 1981-2000, except for elasticity which was calculated using data from 1981-2010 to ensure sufficient data for statistical analysis.

Models	Slope of FDC	Summer elasticity	Winter elasticity	ACF (1)	ACF (2)
GWM0	-0.18	0.36	0.76	0.57	0.44
GWM1	-0.75	-0.02	0.72	0.93	0.16
GWM2	-2.48	0.32	0.72	0.53	0.28
GWM3	-1.40	0.38	-1.36	-0.84	-0.28
GWM4	-0.11	-1.06	-11.03	0.11	-0.26
GWM5	-0.55	0.01	0.67	-0.53	-0.32
δHBV2	0.55	0.76	0.79	0.52	0.71

Table S4 | Median performance metrics at daily scale for LSTM, δHBV1.0, and δHBV2.0 across different continents.
Metrics are based on 4,746 training basins smaller than 50,000 km^2. Bold font indicates the best value in each category. See Table S9 for definitions of each metric.

Region	Model	NSE	KGE	Bias (mm/day)	RMSE (mm/day)	FLV	FHV	Low RMSE (mm/day)	High RMSE (mm/day)
Global	LSTM	**0.732**	0.734	-0.018	0.637	27.035	-12.854	**0.063**	1.541
	δHBV1	0.657	0.662	-0.025	0.732	25.054	-15.225	0.066	1.830
	δHBV2	0.727	**0.742**	0.02	0.657	37.731	**-8.251**	0.068	**1.442**
Europe	LSTM	**0.682**	**0.699**	-0.042	0.499	18.052	-17.360	**0.065**	1.160
	δHBV1	0.574	0.610	-0.042	0.545	15.076	-20.135	0.069	1.447
	δHBV2	0.648	0.696	0.02	0.506	36.537	**-13.547**	0.085	**1.105**

North America	LSTM	0.783	0.787	-0.016	0.786	25.960	-11.007	0.056	1.781
	δHBV1	0.718	0.727	-0.04	0.894	22.334	-15.108	0.05	2.159
	δHBV2	**0.788**	**0.799**	0.003	0.778	29.27	**-6.817**	**0.048**	**1.598**
Africa	LSTM	0.438	**0.381**	-0.032	0.467	219.847	-36.081	0.046	1.388
	δHBV1	0.380	0.249	-0.052	0.503	104.963	-49.526	0.03	1.922
	δHBV2	**0.453**	0.362	-0.044	0.481	59.989	-41.013	0.016	1.564
South Asia	LSTM	**0.745**	**0.783**	-0.118	2.140	8.751	-7.821	0.234	4.628
	δHBV1	0.595	0.610	-0.478	2.743	-30.628	-19.002	0.520	7.244
	δHBV2	0.711	0.755	0.054	2.246	17.661	-6.85	0.269	4.830
Oceania and South Asian Islands	LSTM	0.700	**0.661**	0.015	0.465	160.734	-1.705	0.032	1.600
	δHBV1	0.620	0.484	0.064	0.562	449.635	-2.209	0.062	1.847
	δHBV2	0.700	0.630	0.025	0.508	94.063	2.291	0.021	1.684
South America	LSTM	**0.658**	**0.681**	0.067	0.686	41.938	-11.342	0.138	1.616
	δHBV1	0.551	0.586	0.194	0.829	33.523	-3.497	0.120	1.564
	δHBV2	0.597	0.638	0.208	0.755	50.423	-2.063	0.171	1.448

Table S5 | Summary of global observations datasets.
***A** detailed description can be found in Ather et al[1].*

Variable	Data Source	Number of stations/spatial resolution	Reference/URL
streamflow	ADHI	1466	Tramblay et al.[2]
	BOM Australia	2330	www.bom.gov.au/waterdata/
	CAMELS	4442	Chagas et al.[3], Hoge et al.[4]. Alvarez-Garreton et al.[5] , Coxon et al.[6], Mangukiya et al.[7], Loritz et al.[8]
	CCAM	102	Hao et al.[9]
	Czech Republic	484	https://isvs.chmi.cz/
	Denmark	994	https://odaforalle.au.dk/login.aspx
	Finland	239	www.bom.gov.au/waterdata/
	France	1469	www.hydro.eaufrance.fr
	GRDC	3631	https://portal.grdc.bafg.de/
	HYSETS	2421	Arsenault et al.[10]
	Ireland	312	https://epawebapp.epa.ie/hydronet#Flow
	Italy	294	www.hiscentral.isprambiente.gov.it
	Japan	696	www.river.go.jp/
	LamaHCE	859	Klingler et al.[11]
	LamaHIce	111	Helgason and Nijssen[12]
	Poland	1287	https://danepubliczne.imgw.pl/
	South Korea	391	https://water.nier.go.kr/
	Spain	889	https://ceh.cedex.es/anuarioforos/demarcaciones.asp
	Sweden	274	www.smhi.se
	Thailand	73	https://hydro.iis.u-tokyo.ac.jp/GAME-T/GAIN-T/routine/rid-river/disc_d.html
	USGS	12004	https://dashboard.waterdata.usgs.gov/app/nwd/en/

Table S6 | Summary of forcings and attributes used in model training and simulation.
The details of each attribute can be found in Song et al.[13]

Variables	Description	Units
P	Daily precipitation from MSWEP	mm/day
Temp	Daily mean temperature from MSWX	°C
PET	Potential daily evapotranspiration obtained using Hargreaves method based on maximal and minimal temperature from MSWX	mm/day
catchment area/upstream area	Upstream area of a MERIT unit basin is used in δHBV2.0 and the gage basin area is used in δHBV1.0	km^2
ETPOT_Hargr	Potential evapotranspiration obtained using the Hargreaves method	mm/year
FW	Fraction of open water data in the Global Lakes and Wetlands Database	1

HWSD_clay	Proportion of clay in soil in the Harmonized World Soil Database (HWSD 1.2 and 2.0)	%
HWSD_gravel	Proportion of gravel in soil in the Harmonized World Soil Database (HWSD 1.2 and 2.0)	%
HWSD_sand	Proportion of sand in soil in the Harmonized World Soil Database (HWSD 1.2 and 2.0)	%
HWSD_silt	Proportion of silt in soil in the Harmonized World Soil Database (HWSD 1.2 and 2.0)	%
NDVI	The Normalized Difference Vegetation Index	-
Porosity	Porosity from the Global Hydrogeology Maps (GLHYMPS)	-
SoilGrids_clay	Proportion of clay in the SoilGrids dataset	%
SoilGrids_sand	Proportion of clay in the SoilGrids dataset	%
SoilGrids_silt	Proportion of clay in the SoilGrids dataset	%
aridity	Aridity calculated from forcings	-
glaciers	Glacier fraction from the Global Lithological Map (GLiM)	1
meanP	Mean precipitation from WorldClim	mm/year
meanTa	Mean temperature from WorldClim	°C
Mean elevation	Mean elevation	m
meanslope	Mean slope	degree
permafrost	Permafrost	1
permeability	Permeability from the Global Hydrogeology Maps (GLHYMPS)	$\log(m^2)$
seasonality_P	Precipitation seasonality index calculated using the Seasonality Index (SI) method	-
seasonality_PET	Potential Evapotranspiration seasonality index calculated using the Seasonality Index (SI) method	-
snow_fraction	Snow fraction	1
snowfall_fraction	Snowfall fraction	1

Note: All climate forcings are provided at 0.1° spatial and daily temporal resolution, and attribute data were static and resampled accordingly.

Table S7 | HBV module details, including their equations, fluxes, and parameters.

Modules	Equations	Fluxes	Parameters
Snow accumulation and melt	$\frac{dS_{\mathrm{p}}}{dt} = P_{\mathrm{s}} + R_{\mathrm{fz}} - S_{\mathrm{melt}}$ $P_{\mathrm{s}} = P$ if $T < \theta_{\mathrm{TT}}$, otherwise 0 $R_{\mathrm{fz}} = (\theta_{TT} - T)\theta_{\mathrm{DD}}\theta_{\mathrm{rfz}}$ $s_{\mathrm{melt}} = (T - \theta_{\mathrm{TT}})\,\theta_{\mathrm{DD}}$ $\frac{dS_{\mathrm{liq}}}{dt} = s_{\mathrm{melt}} - R_{\mathrm{fz}} - I_{\mathrm{snow}}$ $I_{\mathrm{snow}} = s_{\mathrm{liq}} - \theta_{\mathrm{CWH}} S_{\mathrm{p}}$	S_{p}: storage in snow P_{s}: precipitation as snow R_{fz}: refreezing of liquid snow S_{melt}: snowmelt as water equivalent S_{liq}: liquid water content in the snowpack I_{snow}: snowmelt infiltration to soil moisture	θ_{TT}: threshold temperature for snowfall [°C], range: [-2.5,2.5]. θ_{DD}: degree-day factor [mm°C^{-1}day^{-1}], range: [0,0.1]. θ_{rfz}: refreezing coefficient [-], range: [0.5,10]. θ_{CWH}: water holding capacity as a fraction of the current snowpack [-], range: [0,0.2].
Soil moisture and evapotranspiration	$\frac{dS_{\mathrm{S}}}{dt} = I_{\mathrm{snow}} + P_{\mathrm{r}} - P_{\mathrm{eff}} - E_x - E_T(+C_r)$ $P_{\mathrm{r}} = P$ if $T > \theta_{\mathrm{TT}}$ otherwise 0 $P_{\mathrm{eff}} = \min\left(\left(\frac{S_{\mathrm{S}}}{\theta_{\mathrm{FC}}}\right)^{\beta}, 1\right)(P_{\mathrm{r}} + I_{\mathrm{snow}})$ $E_x = (S_{\mathrm{S}} - \theta_{\mathrm{FC}})/dt$ $E_T = \min\left(\left(\frac{S_{\mathrm{S}}}{\theta_{\mathrm{FC}}\theta_{\mathrm{LP}}}\right)^{\gamma}, 1\right)E_P$ $C_r = \theta_{\mathrm{C}} * S_{\mathrm{LZ}} * (1 - \frac{S_{\mathrm{S}}}{\theta_{\mathrm{FC}}})$	S_{S} : storage in soil moisture S_{LZ}: current storage in the lower subsurface zone P_{r}: precipitation as rain P_{eff}: effective flow to the upper subsurface zone E_x: rainfall excess E_T: actual evapotranspiration. C_r: an upward flow from the lower subsurface zone. This flux is only used in δHBV1.1p	θ_{C}: time parameter [day^{-1}], range: [0,1]. θ_{FC}: maximum soil moisture (field capacity) [mm], range: [50,1000]. θ_{LP}: vegetation wilting point [-], range: [0.2,1]. β: a parameter influencing the shape of the soil moisture function [-], range: [1,6]. γ: a parameter influencing the shape of the evapotranspiration function [-], range: [0.3,5].
Runoff generation	$\frac{dS_{\mathrm{UZ}}}{dt} = P_{\mathrm{eff}} + E_x - perc - Q_0 - Q_1$ $perc = \min(\theta_{\mathrm{perc}}, S_{\mathrm{UZ}}/dt)$ $Q_0 = \theta_{K_0}(S_{\mathrm{UZ}} - \theta_{\mathrm{UZL}})$ $Q_1 = \theta_{K_1} S_{\mathrm{UZ}}$ $\frac{dS_{\mathrm{LZ}}}{dt} = perc - Q_2(-C_r)$ $Q_2 = \theta_{K_0} S_{\mathrm{LZ}}$ $Q' = Q_0 + Q_1 + Q_2$ $Q_b(t) = \int_0^t \xi(s) Q'(t-s)ds$ $\xi(s) = \frac{1}{\Gamma(\theta_{\mathrm{a}})\theta_{\mathrm{b}}^{\theta_{\mathrm{a}}}} s^{\theta_{\mathrm{a}}-1} e^{-\frac{1}{\theta_{\mathrm{b}}}}$	S_{UZ}: storage in the upper subsurface zone $perc$: percolation to the lower subsurface zone Q_0: near surface flow Q_1: interflow Q_2: baseflow S_{LZ}: storage in the lower subsurface zone Q_b: simulated streamflow for basin b	θ_{perc}: percolation flow rate [mm/day], range: [0,10]. θ_{K_0}(range: [0,10]), θ_{K_1}(range: [0.05,0.9]), and θ_{K_2}(range: [0.001,0.2]): recession coefficients [day^{-1}] θ_{a} (range: [0,2.9]) and θ_{b}(range: [0,6.5]): two routing parameters [-] θ_{UZL}: maximum storage of the upper soil layer [mm], range: [0,100].

Table S8 | Summary of MERIT river attributes used in δMC model training and simulation.

Variables	**Description**	**Units**
len	MERIT river length	km
len_dir	Direct length between starting and ending point	km
sinuosity	len/ len_dir	%
slope	Slope for MERIT river	km^2
stream_drop	TauDEM-calculated stream drop	m
Log_uparea	Log-scale value of the upstream drainage basin in km^2	$log(km^2)$
aridity	The same attributes as δHBV2.0	%

Table S9 | Model evaluation metrics.

Metric	**Equation**	**Description**
NSE	$NSE = 1 - \frac{\sum_{i=1}^{i=N}(Q_i^{obs} - Q_i^{sim})^2}{\sum_{i=1}^{i=N}(Q_i^{obs} - \overline{Q_i^{obs}})^2}$	Ratio of the model error variance to the observed variance, where 1 indicates a perfect model and 0 indicates performance equivalent to predicting with the long-term mean
KGE	$KGE = 1 - \sqrt{(r-1)^2 + (a-1)^2 + (b-1)^2}$	A comprehensive assessment of Pearson's correlation (r), variability (a), and bias (b).
Bias	$Bias = \frac{1}{n}\sum_{i=1}^{n}(Q_i^{sim} - Q_i^{obs})$	Average difference between simulated and observed values
RMSE	$RMSE = \sqrt{\frac{\sum_{i=1}^{i=N}(Q_i^{obs} - Q_i^{sim})^2}{n}}$	Root-mean-square error (RMSE) of runoff
highRMSE	$RMSE = \sqrt{\frac{\sum_{i=1}^{i=N}(Q_i^{obs} - Q_i^{sim})^2}{n}}$	RMSE of the top 2% of the streamflow range
lowRMSE	$RMSE = \sqrt{\frac{\sum_{i=1}^{i=N}(Q_i^{obs} - Q_i^{sim})^2}{n}}$	RMSE of the bottom 30% of the streamflow range
FLV	$FLV = \frac{\sum_{i=1}^{n}(Q_i^{sim\_low} - Q_i^{obs\_low})}{n\sum_{i=1}^{n}(Q_i^{obs\_low})} * 100\%$	Percentile bias of the bottom 30% low flow range
FHV	$FHV = \frac{\sum_{i=1}^{n}(Q_i^{sim\_high} - Q_i^{obs\_high})}{\sum_{i=1}^{n}(Q_i^{obs\_high})} * 100\%$	Percentile bias of the top 2% peak flow range

Supplementary Figures

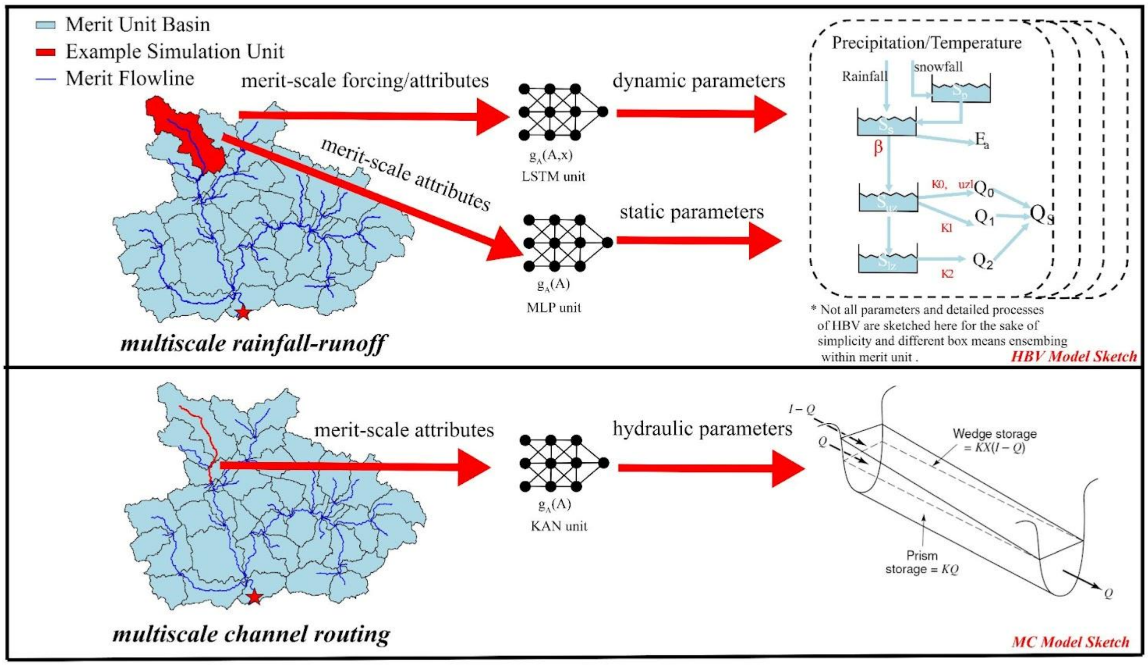

Figure S1 | Sketch of the differentiable model framework.

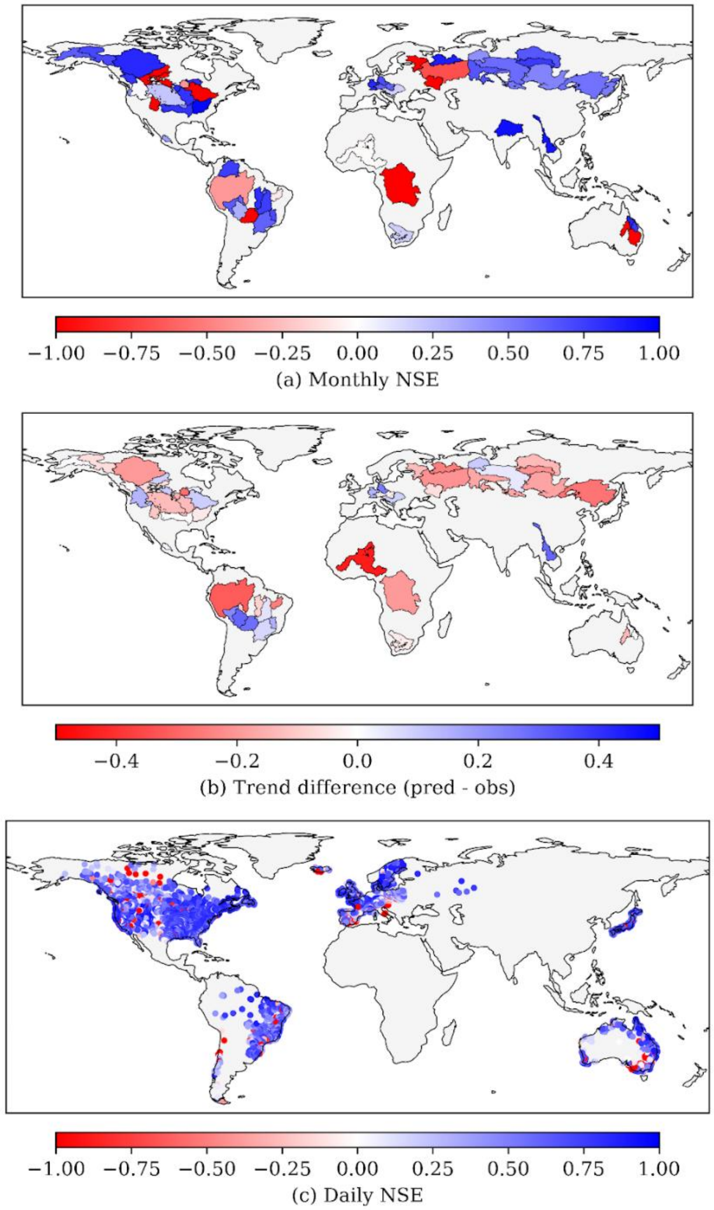

Figure S2 | Nash-Sutcliffe Efficiency (NSE) and trend differences across scales
(a) Monthly NSE of large rivers; (b) difference in trend estimate between observed and simulation (containing all the pairs in Figure 1c and more); and (c) daily NSE of small training and test stations (ds0 + ds1)

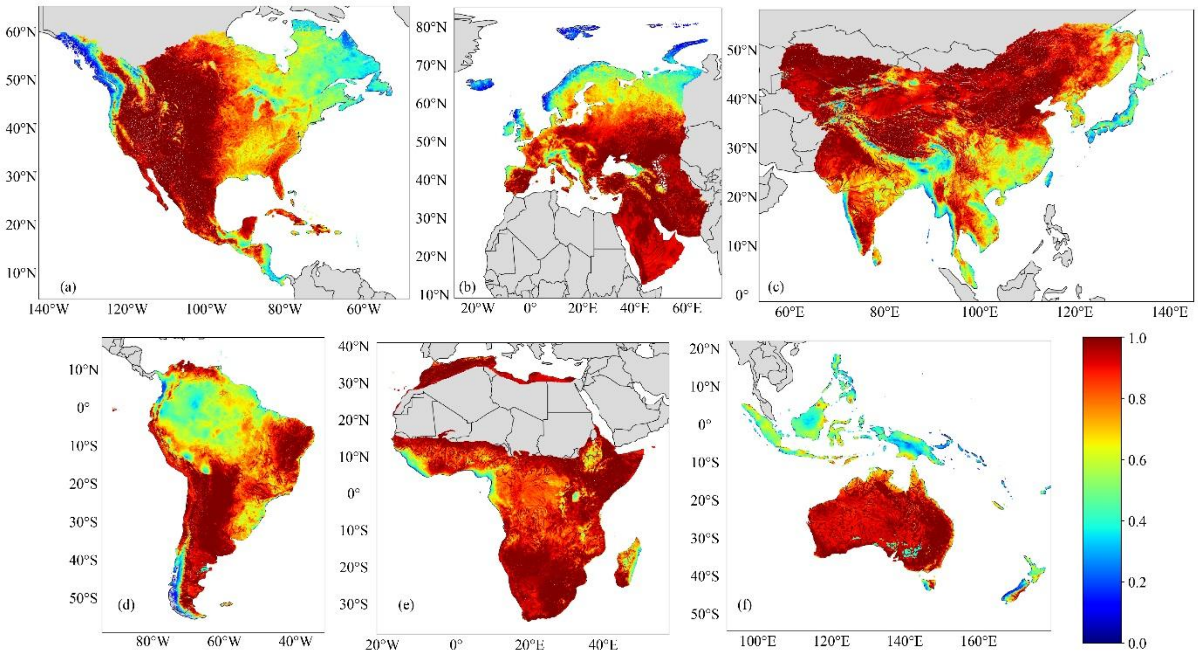

Figure S3 | Distribution of 2001-2020 average ET/P of MERIT unit basins in different continents.
(a) North America; (b) Europe; (c) South Asia; (d) South America; (e) Africa without Sahara Desert; (f) Oceania and South Asian Islands.

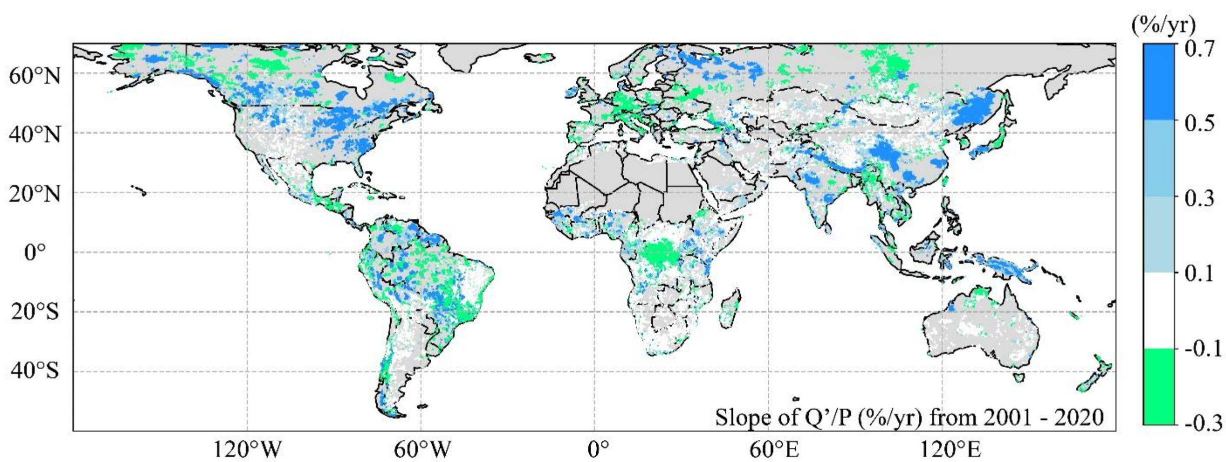

Figure S4 | Temporal trends in annual local runoff to precipitation (Q’/P) ratios from 2001-2020.
Trends are shown as percent change per year in basins with statistically significant trends (Mann-Kendall test, $p < 0.05$ colored).

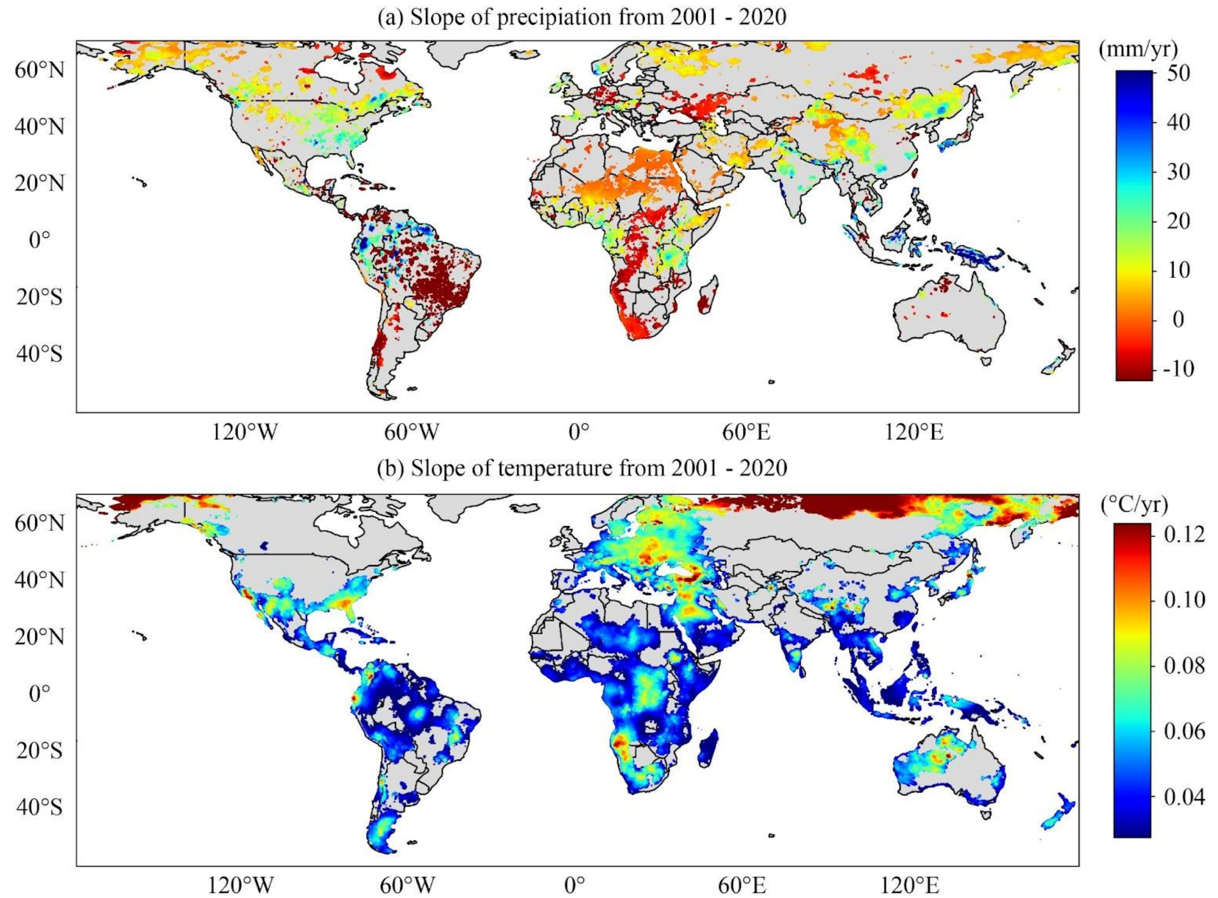

Figure S5 | Decadal-scale precipitation and temperature trends

(a) Decadal-scale trends of precipitation (mm/year) and (b) temperature (℃ /year). Only MERIT unit basins that have statistically significant trends in 2001-2020 in Mann-Kendall test (p < 0.05) are plotted.

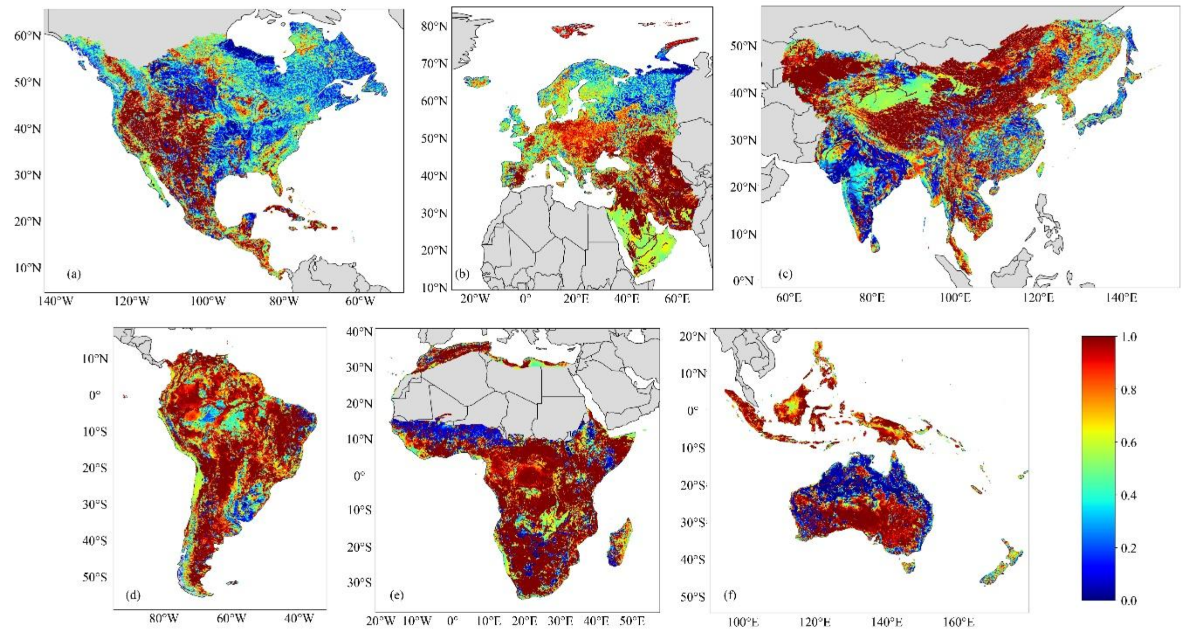

Figure S6 | Distribution of 2001-2020 average baseflow index of MERIT unit basins in different continents.
(a) North America; (b) Europe; (c) South Asia; (d) South America; (e) Africa without Sahara Desert; (f) Oceania and South Asian Islands.

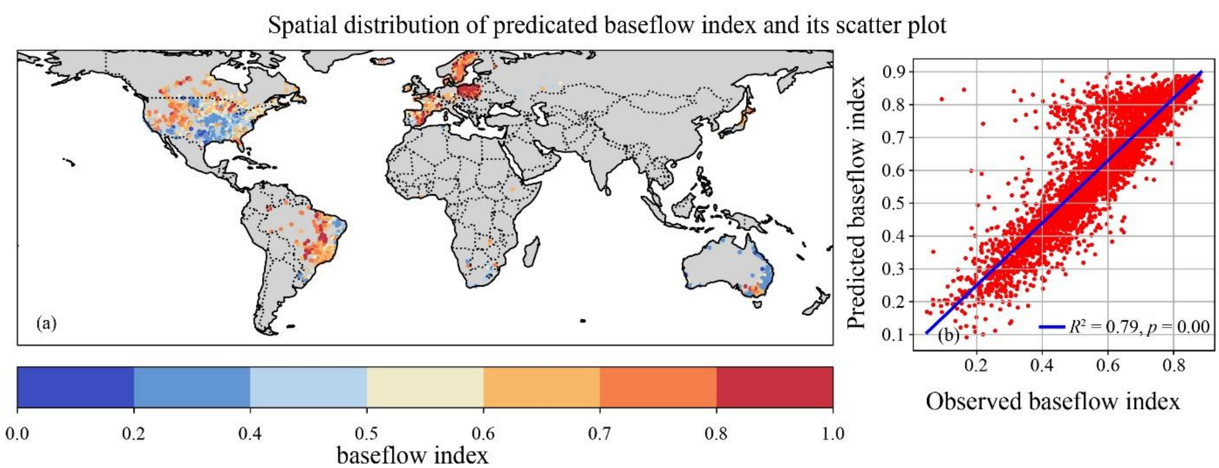

Figure S7 | Spatial distribution and scatter plot of predicted baseflow index.
(a) Gage-based baseflow ratio calculated using our simulated daily streamflow and an ensemble of 12 baseflow-separation methods on the training stations from 1980 to 2015; (b) 1 vs. 1 plot of baseflow ratios calculated based on our simulated flows and observed flows.

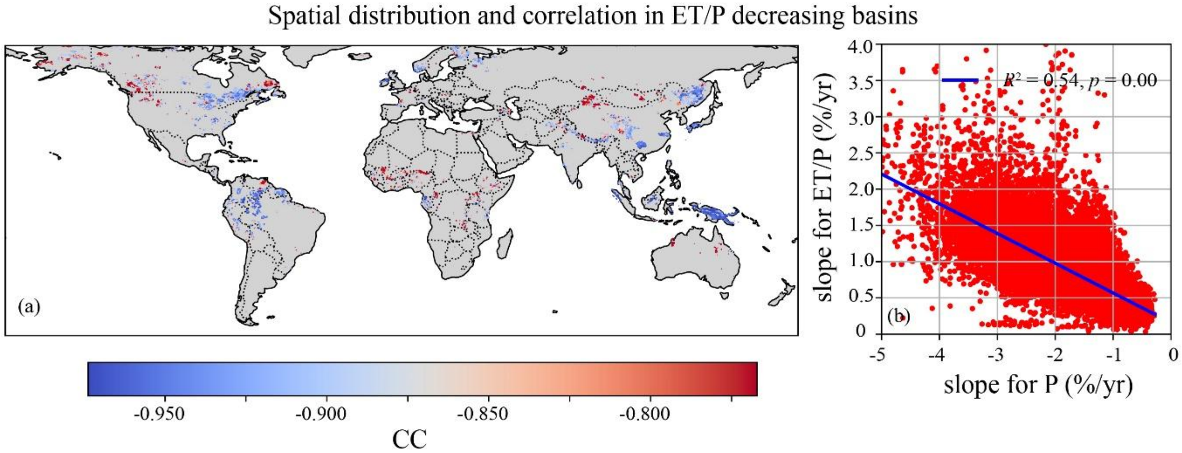

Figure S8 | Spatial distribution and correlation in ET/P decreasing basins.
(a) The temporal correlation coefficient (CC) between annual ET/P and precipitation anomalies, for basins where ET/P has a significant negative trend (same locations as those in Figure 1d), are all negative. (b) The spatial correlation between precipitation change trend in 2001-2020 with the ET/P trend from simulations is also negative, with R^2=0.54. This plot contains basins where the ET/P trend slope ranges from 0 to 4 and exhibits a statistically significant trend (p-value < 0.05).

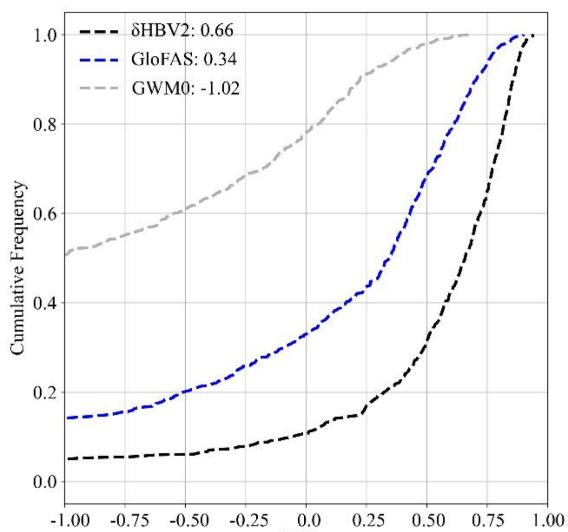

Figure S9 | CDF plots of Nash-Sutcliffe Efficiency (NSE) for δHBV2, GloFAS, and GWM0.
Plots include 664 stations from 1980-01-01 to 2010-12-31. All basins with an area smaller than 50,000km^2, and the area difference between model and observation less than 20% were selected.

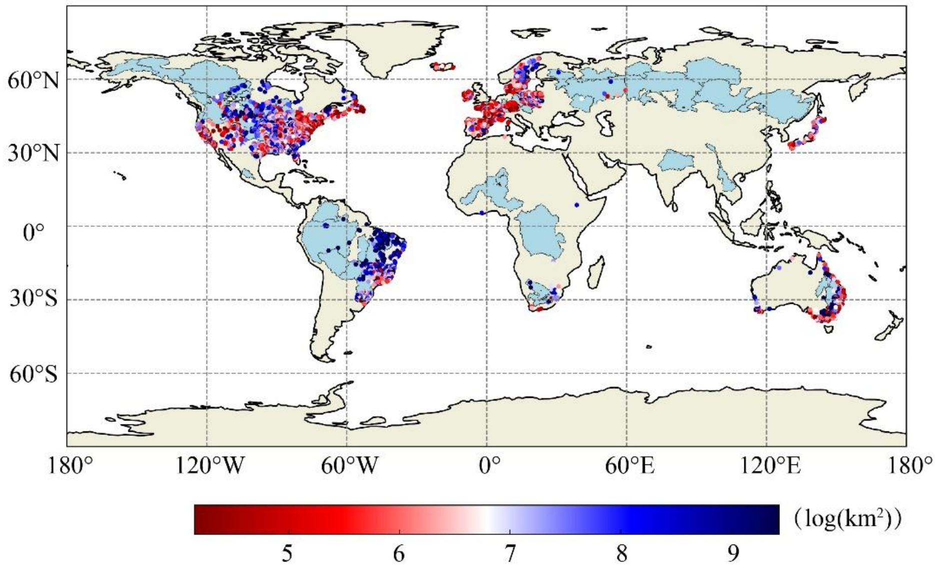

Figure S10 | Locations of 4,746 global training stations.
The color of stations indicates their log-transformed catchment size. The 61 large river basins used for further evaluation are marked as light blue polygons.

Supplementary Text

Text S1: The difference between our baseflow ratio and that in the literature

There are two reasons why our baseflow ratio in Supplementary Figure S5 appears larger than what was presented in the literature. First, prior studies applied baseflow separation to observed daily streamflow, whereas we calculate the ratio by dividing simulated baseflow flux by total simulated runoff, so the concepts are different. Second, our analysis is at the MERIT basin scale, much smaller than typical gaged basins, and hydrologic fluxes are known to be scale-dependent. Finally, if the same baseflow separation method is applied to our simulated streamflow at gage locations, the resulting ratios closely matched those from observed data (Supplementary Figure S6), confirming that the model reproduces realistic baseflow recession behaviors. Our approach thus offers complementary diagnostic insight, and future work could assess which method better reflects actual groundwater contributions.

Text S2: Long Short-Term Memory

LSTM for both streamflow prediction and dynamic parameterization in δHBV share the same structure, including a linear input layer, input, forget, and output gates to selectively add, retain, or discard information, and cell states to maintain short-term and long-term dependencies (Eq. S1 to Eq. S8).

Input transformation:
$$\boldsymbol{x^t} = \mathbf{ReLU}(\boldsymbol{W_{\mathrm{I}}}\boldsymbol{I^t} + \boldsymbol{b_{\mathrm{I}}}) \tag{S1}$$

Input gate:
$$\boldsymbol{i^t} = \boldsymbol{\sigma}(\boldsymbol{\mathcal{D}}(\boldsymbol{W_{\mathrm{ix}}}\boldsymbol{x^t}) + \boldsymbol{\mathcal{D}}(\boldsymbol{W_{\mathrm{ih}}}\boldsymbol{h^{t-1}}) + \boldsymbol{b_{\mathrm{i}}}) \tag{S2}$$

Forget gate:
$$\boldsymbol{f^t} = \boldsymbol{\sigma}(\boldsymbol{\mathcal{D}}(\boldsymbol{W_{\mathrm{fx}}}\boldsymbol{x^t}) + \boldsymbol{\mathcal{D}}(\boldsymbol{W_{\mathrm{fh}}}\boldsymbol{h^{t-1}}) + \boldsymbol{b_{\mathrm{f}}}) \tag{S3}$$

Input node:
$$\boldsymbol{g^t} = \mathbf{tanh}(\boldsymbol{\mathcal{D}}(\boldsymbol{W_{\mathrm{gx}}}\boldsymbol{x^t}) + \boldsymbol{\mathcal{D}}(\boldsymbol{W_{\mathrm{gh}}}\boldsymbol{h^{t-1}}) + \boldsymbol{b_{\mathrm{g}}}) \tag{S4}$$

Output gate:
$$\boldsymbol{o^t} = \boldsymbol{\sigma}(\boldsymbol{\mathcal{D}}(\boldsymbol{W_{\mathrm{ox}}}\boldsymbol{x^t}) + \boldsymbol{\mathcal{D}}(\boldsymbol{W_{\mathrm{oh}}}\boldsymbol{h^{t-1}}) + \boldsymbol{b_{\mathrm{o}}}) \tag{S5}$$

Cell state:
$$\boldsymbol{s^t} = \boldsymbol{g^t} \odot \boldsymbol{i^t} + \boldsymbol{s^{t-1}} \odot \boldsymbol{f^t} \tag{S6}$$

Hidden state:
$$\boldsymbol{h^t} = \mathbf{tanh}(\boldsymbol{s^t}) \odot \boldsymbol{o^t} \tag{S7}$$

Output:
$$\boldsymbol{y^t} = \boldsymbol{W_{\mathrm{hy}}}\boldsymbol{h^t} + \boldsymbol{b_{\mathrm{y}}} \tag{S8}$$

where I^t is the concatenation of the normalized meteorological forcings and static attributes. $\boldsymbol{\mathcal{D}}$ is the dropout operator, which randomly sets the weights of some neurons to zero to prevent overfitting. Variables $\boldsymbol{i}$, $\boldsymbol{f}$, and $\boldsymbol{o}$ are the input, forget, and output gates of LSTM, respectively. $\boldsymbol{g}$ is the input node. $\boldsymbol{s}$ and $\boldsymbol{h}$ represent the hidden states and cell states, respectively. **ReLU, tanh** and $\boldsymbol{\sigma}$ represent the Rectified Linear Unit, the hyperbolic tangent, and sigmoid activation functions, respectively. $\boldsymbol{W}$ and $\boldsymbol{b}$ are the weights of neurons and bias of each layer, respectively. $\odot$ is element-wise multiplication. $\boldsymbol{y}$ is the predicted variable. The predicted variables of the LSTM in δHBV are the HBV parameters, which are further transformed to a range of 0 to 1 using a sigmoid activation function and then rescaled to their actual values based on the parameter ranges provided in Table S7.

Text S3: Model Training and Hyperparameters

In δHBV1.0, LSTM generates time series of all parameters for HBV model, and the static parameters only used the prediction of the last step. In δHBV2, the LSTM and MLP models are trained jointly with the HBV modules, where the LSTM is used for dynamic parameterization and the MLP for static parameterization. In addition, a single LSTM model was also trained separately as a purely data-driven benchmark model for streamflow prediction. All inputs are normalized with Eq. S9. All models in this work used AdamDelta optimizer to automatically adjust the learning rate. LSTM has a hidden size of 256 with a dropout rate of 0.5. MLP has a hidden size of 4096 with a dropout rate of 0.5. The large hidden size for MLP is due to the extensive number of static and routing parameters, its simple structure, and the vast number of MERIT basins[13]. δHBVs were trained to 100 epochs with a batch size of 100. The purely data-driven LSTMs were trained to 300 with a same bath size of δHBVs. δMC used two KANs to estimate the hydraulic parameters and leakage parameters for MC, respectively. KANs used a hidden size of 8. δMC was trained for only 5 epochs with a mini-batch size of 64 basins as its input, as the runoff simulation from δHBV2 is already well-trained.

$$\bar{x}_i = \frac{x_i - \mu_i}{\sigma_i} \tag{S9}$$

where x_i is an input variable of the neural networks; μ_i is the mean value of x_i and σ_i is its standard deviation computed over the entire training dataset.

Text S4: Multilayer Perceptron

The MLP for static parameterization in δHBV2 has the following structure:

$$\begin{aligned} &\text{Input layer:} && \boldsymbol{x_1^t} = \boldsymbol{\mathcal{D}}(\boldsymbol{ReLU}(\boldsymbol{W_I I^t} + \boldsymbol{b_I})) \\ &\text{Hidden layers:} && \boldsymbol{x_i^t} = \boldsymbol{\mathcal{D}}(\boldsymbol{ReLU}(\boldsymbol{W_h x_{i-1}^t} + \boldsymbol{b_h})) \\ &\text{Hidden layer:} && \boldsymbol{y^t} = \boldsymbol{\sigma}(\boldsymbol{ReLU}(\boldsymbol{W_o x_i^t} + \boldsymbol{b_o})) \end{aligned} \tag{S10}$$

where $\boldsymbol{I}$ is the normalized static attributes. $\boldsymbol{W}$ and $\boldsymbol{b}$ with different subscripts are the weights and bias of each layer. There are 6 hidden layers, and $\boldsymbol{x_{i-1}^t}$ in each hidden layer represents the outputs from the previous layer. LSTM and MLP are trained together in δHBV2. Similarly, static and routing parameters predicted by MLP are rescaled to the real parameter values with the parameter ranges provided in Table S7.

Text S5: Kolmogorov-Arnold Networks

The KANs to predict the static Muskingum Cunge parameters in δMC has the following structure:

$$\begin{aligned} &\text{Continuous function:} && \phi_{ij}(x_i) = \alpha_{ij}\boldsymbol{SiLu}(x_i) + \beta_{ij}\sum_i c_i B_i(x_i) \\ &\text{KAN Layer:} && K_j = \sum_{i=1}^{n} \phi_{ij}(x_i) \\ &\text{Output layer:} && \boldsymbol{y} = \boldsymbol{\sigma}(\boldsymbol{K}) \end{aligned} \tag{S11}$$

where x_i is the input of node i in the input layer; subscript j denotes the node j in the output layer. $\sum_i c_i B_i(x_i)$ is the weighted sum of basic functions of all input nodes, where B is the B-spline function and c_i is the weight assigned to node i. The scaling parameter β_{ij} is applied to node i to compute output K_j of the node j in the KAN layer. The $\boldsymbol{SiLu}$ activation function, defined as

$SiLu(x) = x/(1 + e^{-z})$, is employed for non-linearity. c_i, α_{ij} and β_{ij} are trainable parameters. More details about KAN are provided in Liu et al[14].

Text S6: The description about GWM0's bias-correction strategy

GWM0 takes a two-step method to calibrate and bias-correct the rainfall-runoff process. The rainfall-runoff equation in the GWM0 can be described as:

$$R_l = P_{eff}\left(\frac{S_s}{S_{smax}}\right)^{\gamma_l} \tag{S12}$$

The rainfall-runoff exponent, denoted as γ_l, is the only calibratable parameter ranging from 0.3 to 3. This parameter is calibrated with the objective to allow annual mean flow bias to fall within 1% of observation[15]. The calibration is carried out in around 1,300 large basins around the world. All grid points within the calibrated ones will get the same value, while gridcells outside will be extrapolated via a linear regression method with mean annual temperature, mean available soil water capacity, fraction of open water bodies, mean basin land surface slope, fraction of permanent snow and ice, and the aquifer-related groundwater recharge factor as the regressors. If values at the extremes (i.e., γ_l = 0.3 or 3) still result in model underestimation or overestimation it would indicate systematic bias. In that case, a post-simulation linear correction factor was fitted and applied to all grid cells within this basin to achieve the abovementioned 1% bias target. If this correction alone still does not meet the 1% bias criteria, a second adjustment is applied directly to the simulated discharge only at the gauging stations. This secondary incrementally increases or decreases discharge along the flow path from upstream cells to the gauging stations without altering the runoff fields.

References

1. Abbas, A. *et al.* Comprehensive global assessment of 23 gridded precipitation datasets across 16,295 catchments using hydrological modeling. Preprint at https://doi.org/10.5194/egusphere-2024-4194 (2025).
2. Tramblay, Y. *et al.* ADHI: the African Database of Hydrometric Indices (1950–2018). *Earth Syst. Sci. Data* **13**, 1547–1560 (2021).
3. Chagas, V. B. P. *et al.* CAMELS-BR: hydrometeorological time series and landscape attributes for 897 catchments in Brazil. *Earth Syst. Sci. Data* **12**, 2075–2096 (2020).
4. Höge, M. *et al.* CAMELS-CH: hydro-meteorological time series and landscape attributes for 331 catchments in hydrologic Switzerland. *Earth Syst. Sci. Data* **15**, 5755–5784 (2023).
5. Alvarez-Garreton, C. *et al.* The CAMELS-CL dataset: catchment attributes and meteorology for large sample studies – Chile dataset. *Hydrol. Earth Syst. Sci.* **22**, 5817–5846 (2018).
6. Coxon, G. *et al.* CAMELS-GB: Hydrometeorological time series and landscape attributes for 671 catchments in Great Britain. (2020) doi:10.5194/essd-2020-49.
7. Mangukiya, N. K. *et al.* CAMELS-IND: hydrometeorological time series and catchment attributes for 228 catchments in Peninsular India. *Earth Syst. Sci. Data* **17**, 461–491 (2025).
8. Loritz, R. *et al.* CAMELS-DE: hydro-meteorological time series and attributes for 1555 catchments in Germany. Preprint at https://doi.org/10.5194/essd-2024-318 (2024).
9. Hao, Z. *et al.* CCAM: China Catchment Attributes and Meteorology dataset. *Earth Syst. Sci. Data* **13**, 5591–5616 (2021).
10. Arsenault, R. *et al.* A comprehensive, multisource database for hydrometeorological modeling of 14,425 North American watersheds. *Sci Data* **7**, 243 (2020).

11. Klingler, C., Schulz, K. & Herrnegger, M. LamaH-CE: LArge-SaMple DAta for Hydrology and Environmental Sciences for Central Europe. *Earth Syst. Sci. Data* **13**, 4529–4565 (2021).
12. Helgason, H. B. & Nijssen, B. LamaH-Ice: LArge-SaMple DAta for Hydrology and Environmental Sciences for Iceland. *Earth Syst. Sci. Data* **16**, 2741–2771 (2024).
13. Song, Y. *et al.* High-resolution national-scale water modeling is enhanced by multiscale differentiable physics-informed machine learning. *Water Resour. Res.* **61**, e2024WR038928 (2025).
14. Liu, Z. *et al.* KAN: Kolmogorov-Arnold Networks. Preprint at https://doi.org/10.48550/arXiv.2404.19756 (2024).
15. Müller Schmied, H. *et al.* Sensitivity of simulated global-scale freshwater fluxes and storages to input data, hydrological model structure, human water use and calibration. *Hydrol. Earth Syst. Sci.* **18**, 3511–3538 (2014).